

A Permittivity Measurement Method Based on Back Propagation Neural Network by Microwave Resonator

Hong-Gang Hao^{*}, De-Xu Wang, and Zhu Wang

Abstract—In order to solve the problem of the poor performance of the traditional microwave resonance method in multi-parameter fitting data processing, a permittivity measurement method based on Back Propagation (BP) Neural Network algorithm is proposed, which introduces the Neural Network algorithm in data processing of microwave resonance method for the first time. In order to verify the effectiveness of this method in measuring permittivity, a microstrip line structure is used as a microwave resonator. It achieves high sensitivity (4.62%) by loading periodically arranged open resonant rings. On this structure, the reflection coefficients S_{11} of different material samples are simulated as the data of Neural Network. The amplitude and phase of S_{11} and resonant frequency f are taken as the input layer of the Neural Network, respectively. The dielectric constant and dielectric loss are taken as the output to establish the Neural Network model. The simulated and measured results show that the dielectric constant and dielectric loss calculated by the model are basically consistent with the data provided by the manufacturer. The relative error of the dielectric constant is less than 0.6%, and the error of the dielectric loss is less than 0.0005. Compared with the traditional data processing of microwave resonance method, the introduction of BP Neural Network algorithm can significantly improve the accuracy of dielectric constant measurement.

1. INTRODUCTION

Permittivity is an important characteristic parameter of electromagnetic materials [1–3], and its accurate determination plays an important role in medical, industrial, chemical, and biological fields [4, 5]. At present, the microwave resonance method is usually used to measure the permittivity, which uses the measured scattering parameters to solve the complex permittivity by digital fitting or equation [6–8]. In this method, the desired permittivity is first converted into microwave-related electromagnetic parameters that can be measured by the sensor, such as S parameter or resonant frequency offset. The relationship between the dielectric constant and the measured electromagnetic parameters is established by linear fitting or polynomial fitting, which could provide the dielectric constant by any given electromagnetic parameters [9–11]. However, this method can only fit a single electromagnetic parameter, such as the relationship between the resonance frequency and dielectric constant or the quality factor and dielectric loss [12, 13]. It is worth noting that the amplitude, phase, and other data of S parameter could improve the accuracy of the measurement of the complex permittivity. It is difficult for the traditional data fitting method to consider the influence of multiple parameters on the dielectric constant at the same time. The equation method also needs a complex conversion for S parameter to get a multi-parameter transcendental equation [14–16], which increases the calculation amount and uncertainty of measurement. Therefore, it is of great significance in improving the measurement accuracy by using more parameters. In recent years, with the development of artificial intelligence,

Received 7 January 2021, Accepted 7 February 2021, Scheduled 16 February 2021

^{*} Corresponding author: Hong-Gang Hao (haohg@cqupt.edu.cn).

The authors are with the College of Electronic Engineering, Chongqing University of Posts and Telecommunications, Chongqing 400065, China.

Neural Network has become an effective tool in the field of microwave [17–19]. Because of its strong nonlinear fitting ability, Neural Network has become a tool for data processing in this paper.

In view of the limitation of traditional microwave resonance method in data processing, this paper presents a permittivity measurement method based on Back Propagation (BP) Neural Network algorithm. A microstrip line structure based on open resonant ring (SRR) is designed to measure the dielectric constant with S parameters. Through the Neural Network algorithm, we use S parameters in training the Neural Network, which could provide the relationship between the S parameters and dielectric constant of the material under test (MUT). The introduction of BP Neural Network simplifies the process of permittivity data processing and realizes the simultaneous calculation of multiple parameters while improving the accuracy of permittivity.

2. ANALYSIS OF THEORY

The principle of measuring the change of the dielectric constant of the microwave resonant structure is placing the sample at the strongest electric field of a microwave resonant device. When the dielectric constant of the sample is varied, the resonant frequency of the device changes accordingly. The relationship between the dielectric constant and resonance frequency is established by obtaining the resonant frequency of the object with known dielectric constant. Based on the relationship acquired, we could calculate the dielectric constant of the sample through its resonant frequency.

The Neural Network algorithm is applied to the data processing stage of permittivity measurement. The principle is to use a large number of known permittivity media S parameters to train the Neural Network, and then use the trained Neural Network to analyze and measure the permittivity of unknown media. The Neural Network method combines microwave method and big data analysis method, which simplifies the measurement difficulty. With strong nonlinear fitting ability, this method has high flexibility, and it is suitable for multi-parameter simultaneous fitting.

The topology of BP Neural Network algorithm is shown in Fig. 1. Structurally, this is a typical multi-layer structure, which mainly consists of three parts: input layer, hidden layer, and output layer. In general, most of the problems can be solved with one hidden layer, which could avoid the large-scale operation caused by multiple layers while improving the operation efficiency of the algorithm.

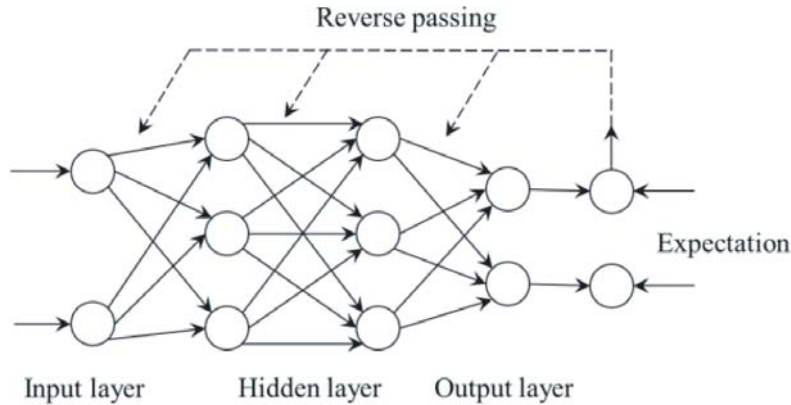


Figure 1. The topology of BP Neural Network algorithm.

The most prominent feature of BP Neural Network model is forward transmission through signals, and when the actual output and predicted output error are higher than the threshold value, the output is transmitted back to the next layer. In the whole transmission process, the neuronal activities in each layer only affect the neurons in the next layer. The weights of each part in the Neural Network can be adjusted and optimized continuously according to the errors between the actual and predicted values in the operation process, until the errors between the output value and the predicted value meet the preset threshold.

The training process of Neural Network is roughly divided into the following stages:

Step 1: Determine the input sample for the Neural Network $P_k = (a_1^k, a_2^k, \dots, a_n^k)$ and target sample $T_k = (s_1^k, s_2^k, \dots, s_p^k)$.

Step 2: Assign the system connection weight ω_{ij} , v_{jt} and threshold θ_j , γ_t randomly in the interval of $(-1, 1)$. Initialize the network and preset iteration times and error conditions.

Step 3: Calculate the input S_j of each unit in the hidden layer by using data such as input sample, system connection weight, and threshold value. The calculation formula is as follows:

$$S_j = \sum_{i=1}^n \omega_{ij} a_i - \theta_j, \quad j = 1, 2, \dots, p \quad (1)$$

The appropriate Neural Network transfer function is selected to calculate the output b_j of each unit in the hidden layer, and the specific form is shown in Equation (2).

$$b_j = f(S_j), \quad j = 1, 2, \dots, p \quad (2)$$

Step 4: Solve the output value C_t of the output unit by existing parameters. The calculation formula is as follows:

$$L_t = \sum_{j=1}^p v_{jt} b_j - \gamma_t, \quad t = 1, 2, \dots, q \quad (3)$$

$$C_t = f(L_t), \quad t = 1, 2, \dots, q \quad (4)$$

Step 5: Compare the output value with the target sample, and Equation (5) is used to calculate the general error d_t^k of each unit in the output layer of Neural Network.

$$d_t^k = (y_t^k - C_t) \cdot C_t(1 - C_t), \quad t = 1, 2, \dots, q \quad (5)$$

Step 6: Calculate the generalized errors e_j^k of each cell in the hidden layer by using Equation (6).

$$e_j^k = \left[\sum_{t=1}^q d_t \cdot v_{jt} \right] \cdot b_j(1 - b_j) \quad (6)$$

Step 7: Fix system connection weights and thresholds by d_t^k and b_j .

$$v_{jt}(N+1) = v_{jt}(N) + \alpha \cdot d_t^k \cdot b_j \quad (7)$$

$$\gamma_t(N+1) = \gamma_t(N) + \alpha \cdot d_t^k, \quad t = 1, 2, \dots, q, \quad j = 1, 2, \dots, p \quad (8)$$

Step 8: Modify system connection weights and thresholds by e_j^k and input sample.

$$\omega_{ij}(N+1) = \omega_{ij}(N) + \beta \cdot e_j^k \cdot a_i^k \quad (9)$$

$$\theta_j(N+1) = \theta_j(N) + \beta \cdot e_j^k, \quad i = 1, 2, \dots, n, \quad j = 1, 2, \dots, p \quad (10)$$

Step 9: Go back to Step 3, and substitute the modified system connection weight v_{jt} and threshold γ_t for the forward calculation again. Samples complete the iterations as the accuracy satisfies the requirement. When all samples meet the preset accuracy requirements, the data and Neural Network training will be completed. Otherwise, the iteration will continue until the requirements are met.

3. DEVICE STRUCTURE AND SIMULATION

Figure 2 shows the structure of the microwave resonator.

Rogers 5880 with a relative dielectric constant of 2.2 and dielectric loss ($\tan \delta$) of 0.0009 is selected as the dielectric substrate. The bottom layer of the substrate is covered with copper, and the center of the top layer is a 50 Ohm microstrip line. There are periodically arranged SRR structures on both sides of the microstrip line.

SRR is a basic metamaterial unit structure, which can satisfy the miniaturization design due to its high quality factor. In the field of microwave measurement, SRR plays an important role in improving

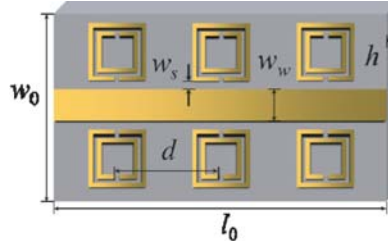


Figure 2. Structure of microwave resonator. The dimensions are as follows: $l_0 = 40$ mm, $w_0 = 20$ mm, $w_w = 1.4$ mm, $w_s = 1$ mm, $d = 9$ mm, $h = 0.787$ mm.

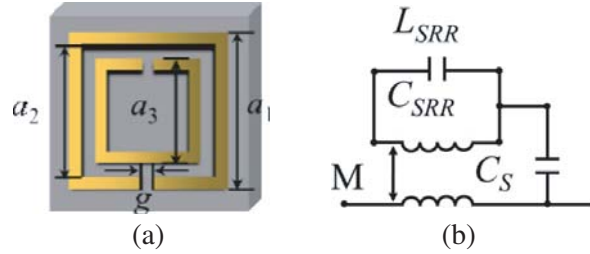


Figure 3. (a) Structure of SRR. (b) Equivalent circuit of SRR. The dimensions are as follows: $a_1 = 3.4$ mm, $a_2 = 3.4$ mm, $a_3 = 2.8$ mm and $g = 0.7$ mm.

the sensitivity and accuracy of sensors. Fig. 3(a) and Fig. 3(b) show the structure and equivalent circuit of SRR [20–23].

The resonant frequency of SRR is solved by the basic LC resonance model, as follows [23, 24]:

$$f_{SRR} = \frac{1}{2\pi\sqrt{L_{SRR}(C_{SRR} + C_S)}} \quad (11)$$

where L_{SRR} and C_{SRR} represent the equivalent inductance and capacitance of SRR. C_S is the capacitance between the microstrip line and SRR [23]. The equivalent capacitance and inductance are related to the parameters of the resonance ring itself, and the resonance frequency can be adjusted by adjusting the size parameters of SRR. The equivalent circuit of the microwave resonator loaded with periodic SRR arrangement is shown in Fig. 4.

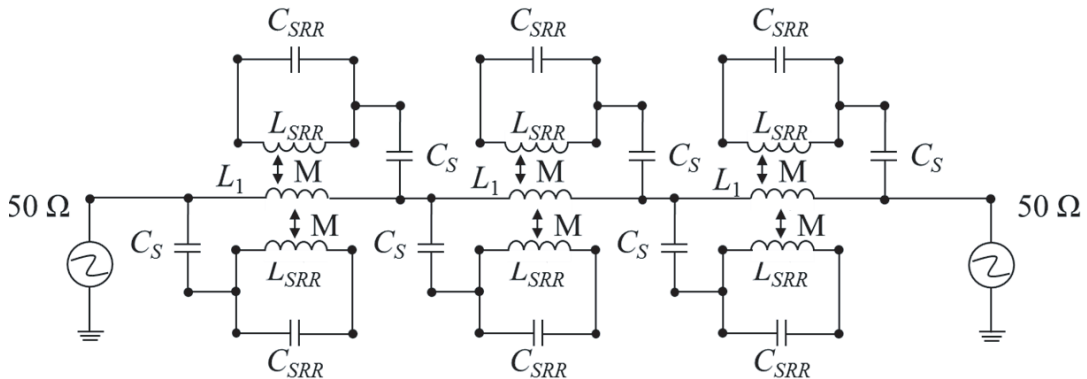


Figure 4. The equivalent circuit of microwave resonator.

The microwave resonance method is based on the changes of resonant frequency to measure the dielectric constant. A larger obvious change of the resonant frequency results in a higher sensitivity of the sensor.

The MUT is placed on the top layer of the resonator and covered with the SRR array. The horizontal dimension of the MUT is 22 mm × 11 mm in order to cover the SRR array, where the electric field distribution is at its maximum, as shown in Fig. 5.

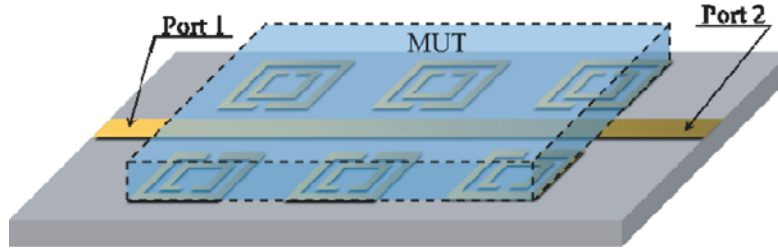


Figure 5. Sample placement state.

The thickness (t_n) of MUT also affects the sensitivity of the sensor. In order to find the appropriate thickness of MUT, the resonant frequency offset (Δf) of sensor under different thicknesses is simulated in HFSS. Fig. 6 shows the frequency offset ($\Delta f = f_{\epsilon'=1} - f_{\epsilon'=10}$) at different thicknesses of the MUT as the permittivity changes from 1 to 10. It may be observed that with the increase of t_n , Δf becomes larger, and the corresponding sensitivity becomes higher. The frequency offset is almost constant for t_n greater than 3 mm. Therefore, the size of the MUT is determined as 22 mm × 11 mm × 3.0 mm.

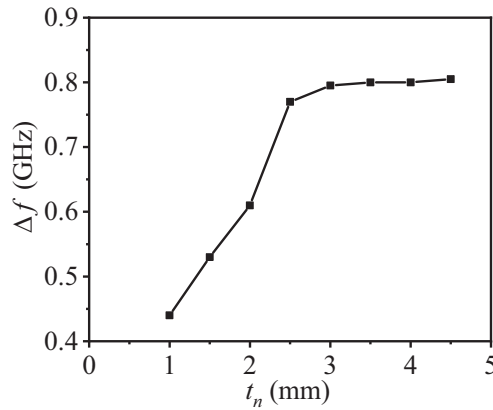


Figure 6. Sample placement state.

In order to show the relationship between dielectric constant and S parameter intuitively, HFSS software is used to simulate the change of the S parameter under different dielectric constants and dielectric losses based on the control variable method. Firstly, we keep the dielectric loss equal to 0.001. The dielectric constant is set as a variable ranging from 1 to 10 (step width 1). The simulation results of reflection coefficient S_{11} are shown in Fig. 7(a). Secondly, the simulation results are obtained under the condition that the dielectric constant is equal to 1 while the dielectric loss varies from 0.001 to 0.01 with a step width of 0.001, which is displayed in Fig. 7(b).

The range of varied dielectric constant and dielectric loss is determined with the consideration of the high dielectric constant and high dielectric loss which dramatically decrease the resonance performance. The range of permittivity is determined to 1–10, and the loss tangent is 0–0.01.

As can be seen from Fig. 6(a), when the MUT dielectric constant changes from 1 to 10, the resonant frequency of the resonator shifts from 2.69 GHz to 1.90 GHz. According to the definition of dielectric constant sensitivity s [25, 26]:

$$s = \frac{\Delta f[\%]}{\Delta \epsilon'} = \frac{f_2 - f_1}{f_1 (\epsilon'_1 - \epsilon'_2)} \quad (12)$$

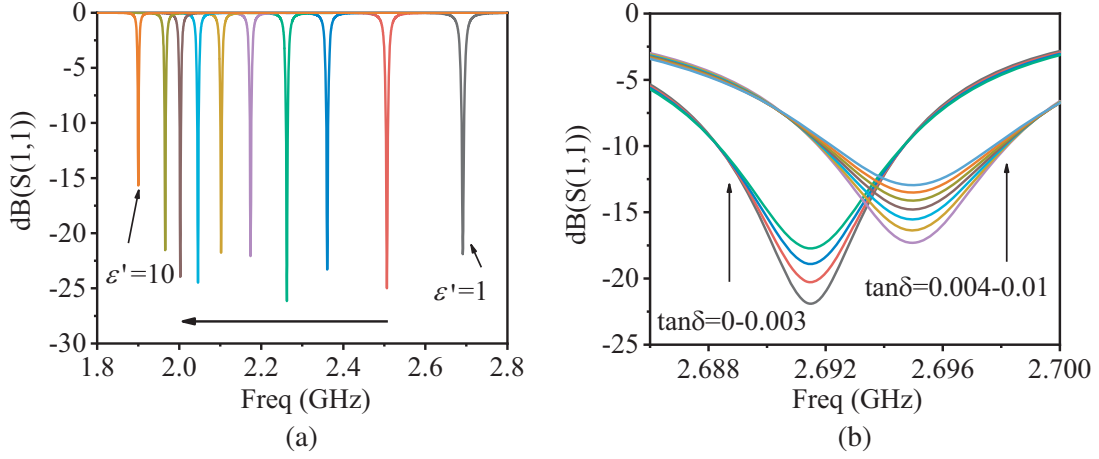


Figure 7. Simulation results of S_{11} . (a) $\tan \delta = 0.001$; $\epsilon' = 1-10$. (b) $\epsilon' = 1$; $\tan \delta = 0-0.01$.

where the resonant frequencies of the sensor with and without MUT are f_1 and f_2 , respectively, while ϵ'_2 and ϵ'_1 represent the dielectric constants with and without MUT, respectively [23]. Based on the results in Fig. 7, the sensitivity of the sensor is 4.62%. Such sensitivity ensures the high reliability of the data measured with the structure.

The resonant frequency corresponding to each dielectric constant and the quality factor under each loss tangent are obtained by Fig. 7. The fitted curves are drawn, as shown in Fig. 8(a).

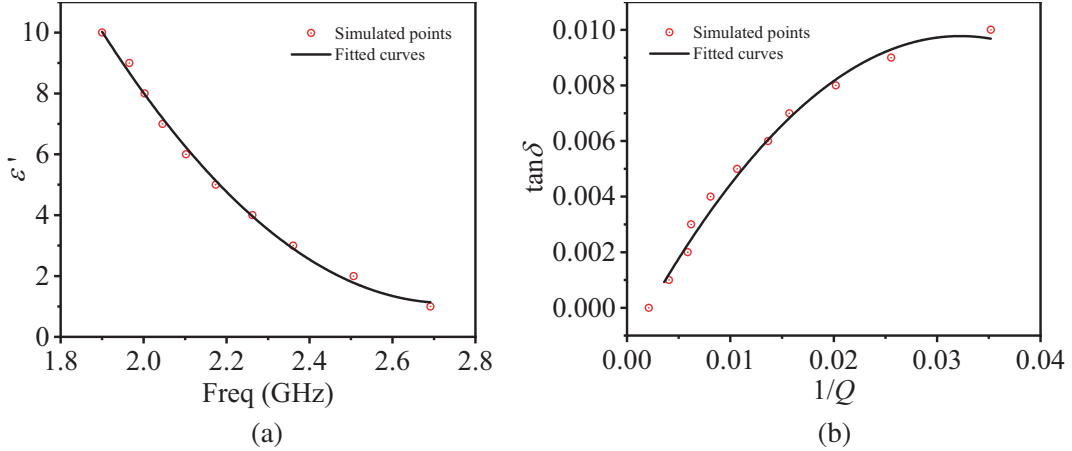


Figure 8. The fitted curves. (a) Resonant frequency with the permittivity. (b) Quality factor with the loss tangent.

The resonant frequency and dielectric constant basically satisfy the quadratic term relation, and the fitting relationship between the dielectric constant and resonance frequency (GHz) is listed as Equation (13). Fitting of the $\tan \delta - 1/Q$ relationship is shown in Fig. 8(b). $\tan \delta$ and $1/Q$ basically agree with the quadratic relationship of Equation (14).

$$\epsilon' = 12.825f^2 - 70.118f + 96.953 \quad (13)$$

$$\tan \delta = -\frac{10.291}{Q^2} + \frac{0.6767}{Q} - 0.0012 \quad (14)$$

According to Equations (13) and (14), the calculation model of the relative dielectric constant under the circuit can be established.

4. NEURAL NETWORK MODEL

In order to obtain the permittivity and $\tan \delta$ of MUT from S parameter, BP Neural Network model is used to establish the relationship between the S parameter and complex permittivity. The 2.6 amplitude and phase of S_{11} and f are respectively taken as the input layer of the Neural Network. ϵ' and $\tan \delta$ are taken as the output. The Neural Networks are trained with 1919 samples of f and S_{11} . While maintaining the measurement selectivity, these samples are acquired when MUT dielectric constant and dielectric loss vary between 1 and 10 (step width 0.5), and 0 and 0.01 (step width 0.0001), respectively. In the process of model building, the samples of odd sequence are used for training Neural Network model, and the samples of even sequence are used for error analysis. The constructed Neural Network structure is shown in Fig. 9.

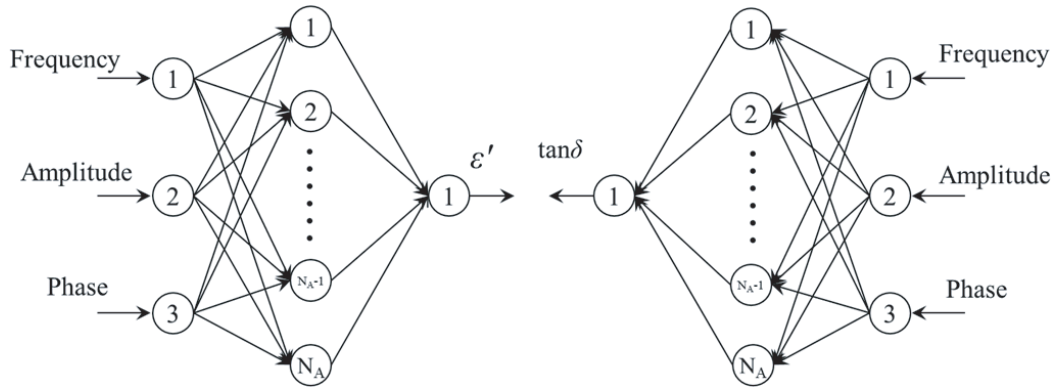


Figure 9. Structure of constructed Neural Network.

As shown in Fig. 9, the Neural Network model has 3 neurons at the input layer, 1 neuron at the output layer and a hidden layer. The number of neurons N_A at the hidden layer is 5. The transfer function of neurons in the hidden layer is tangent function *Tansig*, while the output layer is pure linear function *Purelin*. The training algorithm uses *Levenberg Marquardt* algorithm. The simulation results and errors are shown in Fig. 8.

It can be seen from Fig. 10 that the prediction of ϵ' and $\tan \delta$ by using the established Neural Network model is in good agreement with the expectation, and the measurement results are relatively stable. For the samples used for error measurement, the relative error of dielectric constant of 90% samples is less than 2%, and the error value of dielectric loss of 90% samples is less than 0.0005, indicating a high accuracy.

Figure 11 shows the average error for each set of data. Taking 2% and 0.0005 as the error thresholds of dielectric constant and dielectric loss, respectively, then the measurement ranges of the permittivity and dielectric loss are 1–9 and 0–0.008.

5. EXPERIMENT AND DISCUSSION

Agilent vector network analyser N5242A is used to measure the S parameters. The resonator and measurement system are shown in Fig. 12. Rogers5880 ($\epsilon' = 2.2$, $\tan \delta = 0.0009$), F4B ($\epsilon' = 2.65$, $\tan \delta = 0.001$), Rogers4350 ($\epsilon' = 3.48$, $\tan \delta = 0.004$), FR4 ($\epsilon' = 4.4$, $\tan \delta = 0.004$), and PVC ($\epsilon' = 8.00$, $\tan \delta = 0.005$) are selected as the MUT. These values of dielectric constant and dielectric loss are acquired from the properties of materials in HFSS at 9.4 GHz [8, 11, 26].

The measured results of S parameter are shown in Fig. 13.

For the traditional digital fitting method, Equations (13) and (14) are used to calculate the dielectric constant and dielectric loss of the sample. The maximum relative error of the permittivity reaches 8.64%. The error of dielectric loss is up to 0.00101. Thus, it is necessary to reduce errors in data processing.

The BP Neural Network algorithm is used to calculate the dielectric constant. The frequency f and amplitude and phase of S_{11} are substituted into the BP Neural Network model, and the calculated

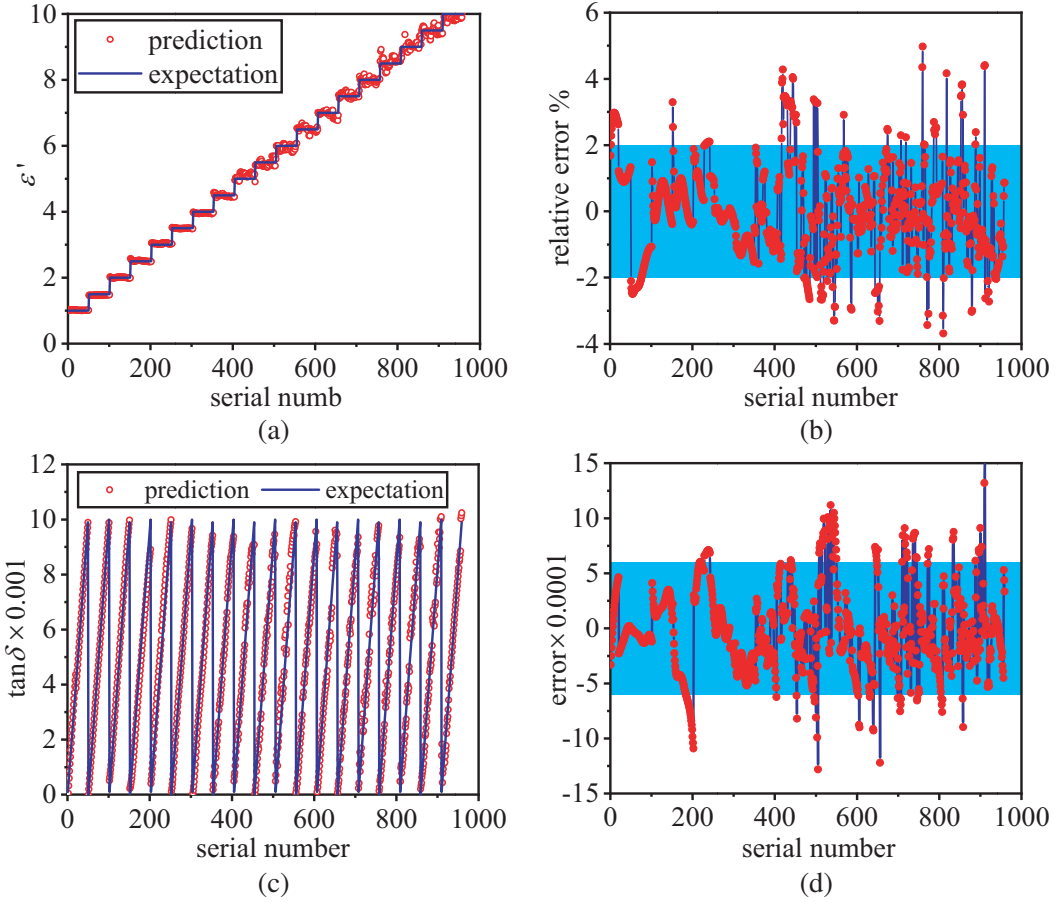


Figure 10. Simulation results. (a) Prediction and expectation of ϵ' . (b) Relative error of ϵ' . (c) Prediction and expectation of $\tan \delta$. (d) Error of ϵ' .

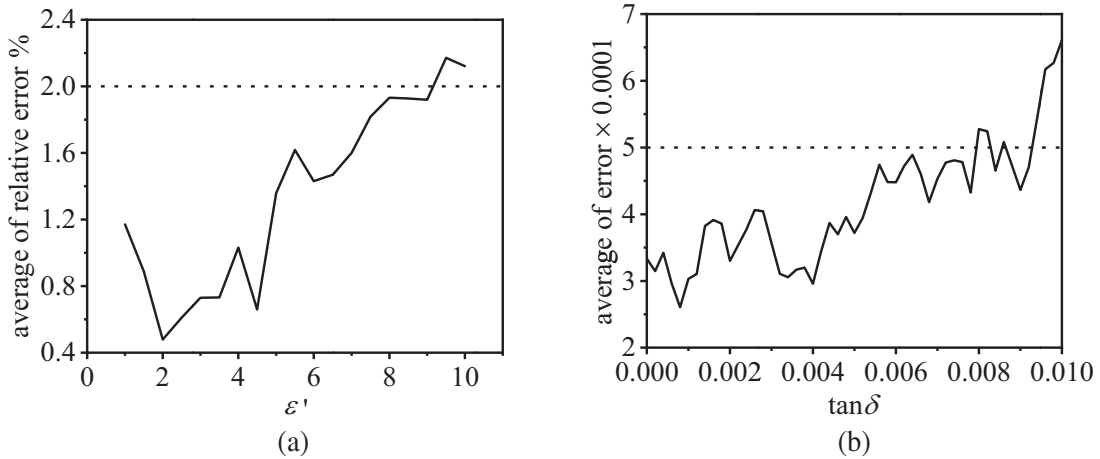


Figure 11. The average error for each set of data. (a) Dielectric constant. (b) Dielectric loss.

permittivity and dielectric loss measurement results and errors are shown in Fig. 14.

The experimental results show that ϵ' and $\tan \delta$ calculated by the model are basically consistent with the data provided by the manufacturer. The relative error of ϵ' is less than 0.6%, and the $\tan \delta$ is less than 0.0005.

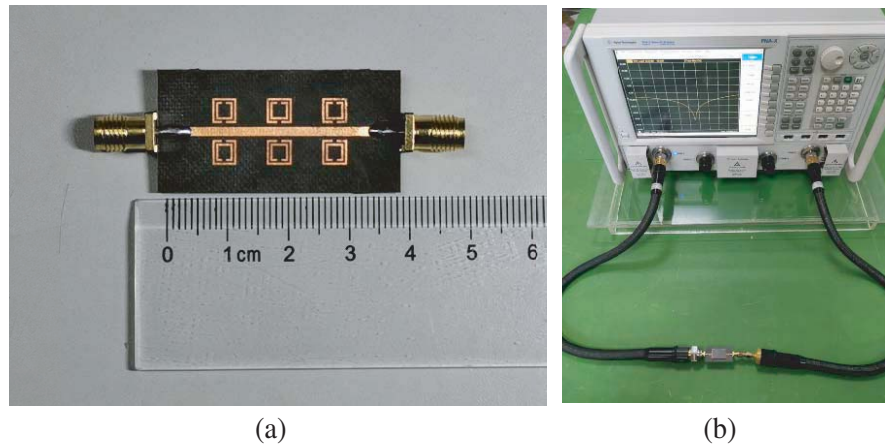


Figure 12. (a) Fabricated microwave resonator. (b) Measurement system.

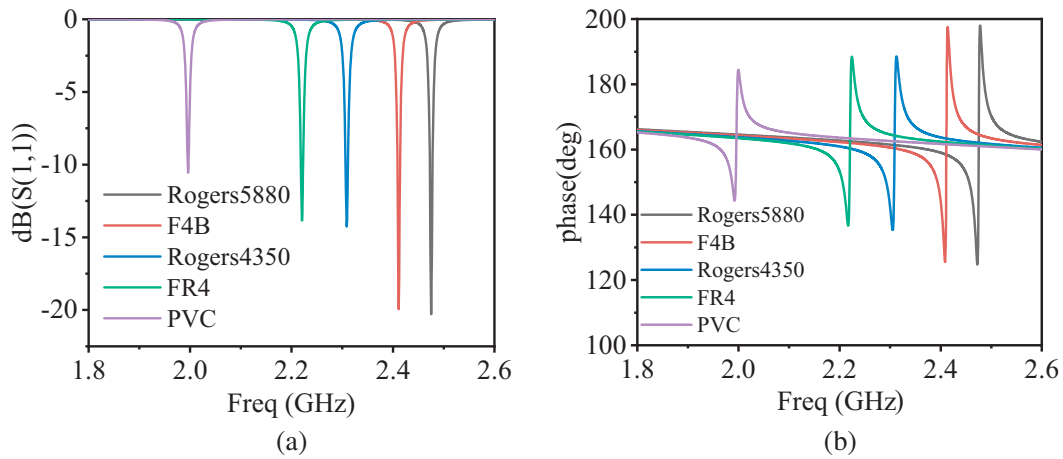


Figure 13. Measurement results of S_{11} . (a) Amplitude of S_{11} . (b) Phase of S_{11} .

The dielectric constants calculated by the traditional data fitting and the BP Neural Network algorithm are compared, and the result is shown in Table 1.

Table 1. The comparison of results for fitted and BP Neural Network.

The MUT	ϵ'			$\tan\delta$		
	Standard	Error% (Fitted)	Error% (BP)	Standard	Error (Fitted)	Error (BP)
Rogers 5880	2.20	8.64%	0.12%	0.0009	0.00098	0.00045
F4B	2.65	7.17%	0.39%	0.001	0.00101	0.00049
Rogers 4350	3.48	1.72%	0.48%	0.004	0.00048	0.00013
FR4	4.40	2.28%	0.56%	0.004	0.00022	0.00015
PVC	8.00	0.25%	0.03%	0.005	0.00027	0.00008

It can be seen from Table 1 that the use of BP Neural Network can indicate a high measurement accuracy. It has a certain degree of reliability.

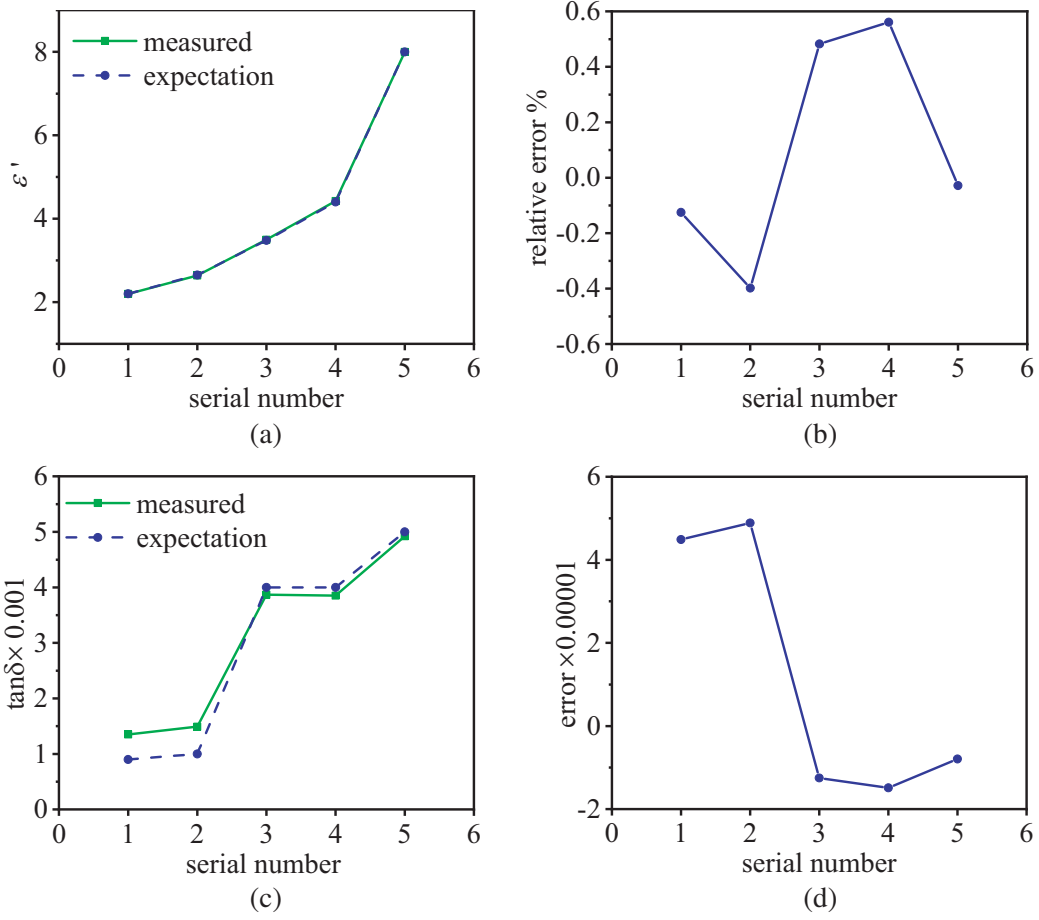


Figure 14. Measurement results. (a) Prediction and expectation of ϵ' . (b) Relative error of ϵ' . (c) Prediction and expectation of $\tan \delta$. (d) Error of ϵ' .

6. ANALYSIS OF ERROR

As can be seen from the experimental results, compared with the traditional method, in data processing, the BP Neural Network is more accurate and easier to measure the permittivity. However, in some frequency points there will be a large error. The error analysis of this method shows that the main reasons for the error are as follows:

First of all, the error caused by the placement position of the MUT. It is worth noting that because the sensor and MUT are both rough planes, it is impossible to achieve complete contact as in the simulation conditions, which is an important source of error in the measurement process. In addition, the location of MUT can also affect the measurement results. In this paper, the average value of multiple measurements is taken to reduce the two kinds of errors as far as possible.

Secondly, the error caused by sample preparation. The sample used for measurement needs to be consistent with the size of simulation, but due to technological limitations, there will be errors between the actual size of the processed sample and the expected size. The method to reduce this error is to obtain high precision standard samples from professional plate manufacturers. The first two errors are evident in the measurement of solid materials. However, these two kinds of errors almost do not exist when using the proposed data treatment to measure the liquid. It is one of the emphases of future research to measure the dielectric constant of liquid by using the experimental method in this paper.

Then, the training data are derived from the simulation results of the simulation software. However, when the actual media are measured, the S parameters which are substituted into the network are

measured data. Therefore, the error between the training data and measured data is the main source of the permittivity measurement error of the Neural Network method. When the measured S parameter is also used in the training data, this error can be greatly reduced, but multiple media with different dielectric constants need to be processed, which increases the cost and complexity of this method. The error can be reduced by decreasing the sampling step and increasing the sampling amount.

Lastly, the errors are also due to sensor plate processing and SMA joint welding process. The error can be reduced by standard sample calibration.

7. CONCLUSION

In this paper, based on the microwave resonance structure loaded with an SRR structure, a measurement method of dielectric constant based on BP Neural Network algorithm is proposed, realizing the measurement of ε' and $\tan \delta$. The measurement ranges of the permittivity and dielectric loss are 1–9 and 0–0.008. The simulation and measurement results show that this method avoids the shortcoming of the traditional method of insufficient nonlinear fitting ability. The Neural Network training of S parameter makes the calculated results more consistent with the standard value of MUT, and the reliability is higher.

REFERENCES

1. Vélez, P., J. Naqui, A. Prieto, M. sindreu, J. Bonache, J. Martel, F. Madina, and F. Martín, "Differential bandpass filter with common-mode suppression based on open split ring resonators and open complementary split ring resonators," *IEEE Microw. Wirel. Components Lett.*, Vol. 23, No. 1, 22–24, Jan. 2013.
2. Karami, M., P. Rezaei, S. Kiani, and R. A. Sadeghzadeh, "Modified planar sensor for measuring dielectric constant of liquid materials," *Electron Lett.*, Vol. 53, No. 19, 1300–1302, Sep. 2017.
3. Xie, Y., F. Shen, T. Zhou, B. Zhang, J. Wang, C. Li, and L. Ran, "Remote measurement of dielectric constants for samples with arbitrary cross sections," *IEEE Microw. Wirel. Components Lett.*, Vol. 30, No. 10, 1005–1008, Oct. 2020.
4. Ye, D., O. Omkar, and P. Wang, "A dual-mode microwave resonator for liquid chromatography applications," *IEEE Sensors Journal*, Vol. 21, No. 2, 1222–1228, 2021.
5. Wu, C., Y. Liu, S. Lu, S. Gruszczynski, and Y. Yashchyshyn, "Convenient waveguide technique for determining permittivity and permeability of materials," *IEEE Trans. Microw. Theory Techn.*, Vol. 68, No. 11, 4905–4912, Nov. 2020.
6. Adhikari, K. K. and N.-Y. Kim, "Ultrahigh-sensitivity mediator-free biosensor based on a microfabricated microwave resonator for the detection of micromolar glucose concentrations," *IEEE Trans. Microw. Theory Techn.*, Vol. 64, No. 1, 319–327, Jan. 2016.
7. Yin, B., Z. Lin, X. Cai, H. Hao, W. Luo, and W. Huang, "A novel compact CRLH bandpass filter on CSRR-loaded substrate integrated waveguide cavity," *Progress In Electromagnetics Research M*, Vol. 75, 121–129, 2018.
8. Gil, M., P. Vélez, F. Aznar-Ballesta, J. Muñoz-Enano, and F. Martín, "Differential sensor based on electroinductive wave transmission lines for dielectric constant measurements and defect detection," *IEEE Trans. Antennas Propag.*, Vol. 68, No. 3, 1876–1886, Mar. 2020.
9. Kayal, S., T. Shaw, and D. Mitra, "Design of metamaterial-based compact and highly sensitive microwave liquid sensor," *Applied Physics A*, Vol. 126, No. 1, 1–9, 2020.
10. Yang, C., C. Lee, K. Chen, and K. Chen, "Noncontact measurement of complex permittivity and thickness by using planar resonators," *IEEE Trans. Microw. Theory Techn.*, Vol. 64, No. 1, 247–257, Jan. 2016.
11. Alahnomi, R. A., Z. Zakaria, E. Ruslan, S. R. Ab Rashid, and A. A. Mohd Bahar, "High-Q sensor based on symmetrical split ring resonator with spurlines for solids material detection," *IEEE Sensors J.*, Vol. 17, No. 9, 2766–2775, May 2017.

12. Sungyun, J., B. S. Izquierdo, and E. A. Parker, "Liquid sensor/detector using an EBG structure," *IEEE Trans. Antennas Propag.*, Vol. 67, No. 5, 3366–3373, May 2019.
13. Vélez, P., J. Muñoz-Enano, K. Grenier, J. Mata-Contreras, D. Dubuc, and F. Martín, "Split Ring Resonator (SRR) based microwave fluidic sensors for electrolyte concentration measurements," *IEEE Sens. J.*, Vol. 19, No. 7, 2562–2569, Apr. 2019.
14. Terán-Bahena, E. Y., S. C. Sejas-García, and R. Torres-Torres, "Permittivity determination considering the metal surface roughness effect on the microstrip line series inductance and shunt capacitance," *IEEE Trans. Microw. Theory Tech.*, Vol. 68, No. 6, 2428–2434, Jun. 2020.
15. Abdolrazzagh, M., S. Khan, and M. Daneshmand, "A dual-mode split-ring resonator to eliminate relative humidity impact," *IEEE Microw. Wirel. Components Lett.*, Vol. 28, No. 10, 939–941, Oct. 2018.
16. Lee, C. S. and C. L. Yang, "Thickness and permittivity measurement in multi-layered dielectric structures using complementary split-ring resonators," *IEEE Sensors J.*, Vol. 14, No. 3, 695–700, Mar. 2014.
17. Arab, M., X. Garros, J. Cluzel, M. Rafik, X. Federspiel, and G. Ghibaudo, "A new direct measurement method of time dependent dielectric breakdown at high frequency," *IEEE Trans. Electron Devices*, Vol. 41, No. 10, 1460–1463, Oct. 2020.
18. Zhang, J., D. Du, Y. Bao, J. Wang, and Z. Wei, "Development of multifrequency-swept microwave sensing system for moisture measurement of sweet corn with deep neural network," *IEEE Trans. Instrum Meas.*, Vol. 69, No. 9, 6446–6454, Sept. 2020.
19. Bonello, J., A. Demarco, I. Farhat, L. Farrugia, and C. V. Sammut, "Application of artificial neural networks for accurate determination of the complex permittivity of biological tissue," *Sensors*, Vol. 20, No. 16, Aug. 2020.
20. Chuma, E. L., Y. Iano, G. Fontgalland, and L. L. Bravo Roger, "Microwave sensor for liquid dielectric characterization based on metamaterial complementary split ring resonator," *IEEE Sensors J.*, Vol. 18, No. 24, 9978–9983, Dec. 2018.
21. Galindo-Romera, G., F. J. Herraiz-Martínez, M. Gil, J. J. Martínez-Martínez, and D. Segovia-Vargas, "Submersible printed split-ring resonator-based sensor for thin-film detection and permittivity characterization," *IEEE Sens. J.*, Vol. 16, No. 10, 3578–3596, May 2016.
22. Lee, C.-S. and C.-L. Yang, "Complementary split-ring resonators for measuring dielectric constants and loss tangents," *IEEE Microw. Wirel. Components Lett.*, Vol. 24, No. 8, 563–565, Aug. 2014.
23. Hao, H., D. Wang, Z. Wang, B. Yin, and W. Ruan, "Design of a high sensitivity microwave sensor for liquid dielectric constant measurement," *Sensors*, Vol. 20, No. 19, Oct. 2020.
24. Su, L., J. Mata-Contreras, P. Vélez, and F. Martín, "Splitter/Combiner microstrip sections loaded with pairs of Complementary Split Ring Resonators (CSRRs): Modeling and optimization for differential sensing applications," *IEEE Trans. Microw. Theory Tech.*, Vol. 64, No. 12, 4362–4370, Dec. 2016.
25. Jafari, F. and J. Ahmadi, "Reconfigurable microwave SIW sensor based on PBG structure for high accuracy permittivity characterization of industrial liquids," *Sens. Actuators A Phys.*, Vol. 283, 386–395, Nov. 2018.
26. Lobato-Morales, H., D. V. B. Murthy, A. Corona-Chavez, J. L. Olvera-Cervantes, J. Martínez-Brito, and L. G. Guerrero-Ojeda, "Permittivity measurements at microwave frequencies using Epsilon-Near-Zero (ENZ) tunnel structure," *IEEE Trans. Microw. Theory Tech.*, Vol. 59, No. 7, 1863–1868, Jul. 2011.